Vol. 03, Iss. 1 (2025) 137-147, DOI: 10.61552/JME.2025.01.011

Journal of Materials and Engineering

www.jme.aspur.rs

Research article

Modelling the geometry constraints on the cleavage fracture toughness in ferritic steels

D. Hariharan[a], K. Duraivelu[b,*]

[a]*Department of Mechanical, Aerospace and Civil Engineering, The University of Manchester, UK,*
[b]*Department of Mechanical Engineering, SRM Institute of Science and Technology, India.*

Keywords:

Cleavage fracture toughness
Local approach to cleavage fracture
Beremin model
Weibull stress
Plastic strains
Geometry effects

* Corresponding author:

K. Duraivelu
E-mail: duraivek1@srmist.edu.in

Received: 16 September 2024
Revised: 28 October 2024
Accepted: 7 December 2024

A B S T R A C T

Assessing the possibility of cleavage fracture at given operating conditions is significant for the design and maintenance of critical engineering components in the energy, infrastructure and manufacturing sectors. Ductile to brittle transition describes the perceptible shift in fracture mode that occurs when temperature decreases, from slow ductile crack formation to quick cleavage. At very low temperatures, it has been demonstrated that local approaches to cleavage fracture developed based on weibull stress as a cleavage crack-driving force, may predict fracture toughness. But capturing the absolute effects of geometry remains a challenge. This article prescribes a new weibull stress formulation model with thinning function, which alters the number of cleavage-initiating features with temperature. It is found that the modified weibull stress is independent of the weibull shape parameter within the investigational error and it might predict the fracture toughness at any specified geometry and temperature without relying upon the empirical fits. The results prove that there is an excellent agreement observable between the experimental and the theoretical characteristic fracture toughness predicted by the modified Beremin model, rather than original Beremin model for the geometry condition of $a/W = 0.2$ & 0.5 *with a single shape parameter at -110°C.*

1. INTRODUCTION

Ferritic steel is broadly utilised for manufacturing stress boundary elements, which include pressure pipes and vessels because of its higher strength and ductility characteristics. At sufficiently low temperatures, it exhibits crack fracture, which might not initially be a problem but could be crucial because of to its service associated material deprivation. e.g., irradiation fragile of reactor vessels, hydrogen fragile of oil and gas pipes. Local approach to cleavage-fracture (LAF) observes crack as a probabilistic event assumed on local fracture criteria for an unsteady critical micro crack in a volume element and examines the probability density distribution

of these micro cracks. Cleavage fracture toughness (CFT) in ferritic steels is highly influenced by three main factors; temperature, geometry of the crack and service history. Particularly, the stress intensity factor that is used to determine the CFT in ferritic steels is dependent on crack size and the structural geometry. Modelling the geometry constraint effects [1] on the CFT can lead to various useful findings. For precise analyses, finite element calculations are necessary to govern the applied conditions in the cracked structure. Among the multitude of characteristics defining their mechanical behaviour, CFT stands out as a critical parameter, governing the material's ability to resist crack propagation and catastrophic failure.

The Beremin model [2] which specifies a microstructural crack-driving force, the weibull stress and the chance of fracture as a weibull distribution, is the foundation for the majority of local methods to cleavage fracture. The shape parameter m, which is related to the shape of the probability distribution of the micro crack sizes, and the scale parameter, which is related to the elastic properties and surface energy of the material, are the two material-dependent parameters that affect the weibull stress. While the Beremin model accurately forecasts CFT on the lower shelf of the Digital to Brittle (DBT) curve, doing so in the DBT temperature regime has shown to be difficult. The scale parameter should rise with temperature and be adjusted to obtain consensus with the experimental data for the material, whereas the shape parameter must be independent of temperature [3]. This is comparable to assuming that the form of the micro crack size distribution remains constant with temperature while the temperature-dependent changes in the elastic properties and surface energy of the material regulate the variation in CFT.

The Beremin model is the primary local approach to look at crack fracture. It is based totally on the concept of the weakest-link theory that means the macroscopic crack failure hinge on the failure of a single originating micro-crack. From the perspective of statistics, the cleavage process can be expressed as an inhomogeneous spatial poisson point process [4]. In this representation, points correspond to cleavage initiators. Extensive experimental investigations into crack fracture within ferritic steels have highlighted the significant influence exerted by Griffith-like micro-cracks. These micro cracks predominantly emerge from the fracture of rigid, brittle particles like carbides positioned along grain limits. The inherently stochastic nature of this localized fracture process has stimulated the evolution of sophisticated probabilistic models. These models aim to establish a more nuanced relationship between macroscopic fracture behaviour and the unpredictable micro-scale occurrences [5].

The research by Ruggieri [6] provided a toughness scaling model based totally on the weibull stress to obtain the effects of changes of the constraint on CFT data. Central to this approach is the understanding of weibull stress σ_w as the underlying probabilistic force driving cracks. This is linked with the requirement that cleavage fracture transpires once weibull stress attains a critical threshold. Calibrating the weibull modulus, denoted as m is a crucial step in applying the LAF methodology, which is based on the weibull stress concept. The scale parameter, represented as σ_u is determined from the σ_w value corresponding to a 63.2% probability of failure, once the value of m is established. Current methods for estimating the weibull stress parameters involve using the toughness scaling model. This method determines the m parameter by analysing Weibull stress trajectories obtained from two distinct crack configurations with differing levels of constraint (for example, a deep notch and a shallow notch SENB specimen). The objective is to identify the m value that effectively adjusts the probability distribution of J_c from one configuration to match the corresponding J_c - distribution from another configuration. This approach eliminates the ambiguity in calibration that arises when relying solely on one set of fracture toughness data.

Even though the approach proposed by Ruggieri et al. [6] has shown effectiveness in predicting crack fracture behaviour in typical structural steels, especially in the DBT region, practical concerns have been raised. This approach necessitates fracture testing of various crack and specimen configurations. This requirement contradicts the usual practice of conducting fracture analysis and defect assessment using conventional fracture specimens, making the calibration of weibull stress parameters utilising two sets of specimens, a complex process. Latest works in this field consist of works by Andrieu et

al [7]. While these procedures share a comparable basis, utilizing a single set of fracture toughness values from high constraint specimens for parameter calibration, they differ in their strategies for estimating m. Cao et al and Qian et al incorporate a simulation to create a substantial dataset of fracture toughness values, attempting to address the uncertainties introduced by the calibration procedure. However, it remains uncertain whether these methods can overcome the issue of non-uniqueness in calibrated parameters, which can subsequently lead to substantial indecisions in the 'm' parameter.

Maria S Yankova et al [8] adopted in their research work, LAF method which includes the statistical data of micro cracks to estimate the failure probability. The reduced probability of crack in general cannot be predicted accurately at the higher temperature and hence during plastic deformation. They conclude that the changes in CFT cannot be captured by changing the deformation of material properties. Alternatively, change to the fraction of particles with a large dependency on the plastic strains is discussed in their study. Claudio Ruggieri and Andrey P Jivkov [9] focused on the recent developments in modeling of cleavage fracture, which is framed with the support of a local approach. They examine the resilient impact of deviations on CFT in terms of the quantity of suitable micro-cracks that successfully regulate unsteady crack propagation through crack. Stress is given on the inclusion of plastic strain effects into the outline. According to the authors, adopting a reformed version of the weibull stress that incorporates the effects of plastic strain seems to improve the agreement between predicted CFT and experimental measurements. Victor S Barbosa and Claudio Ruggieri [10] developed a basic estimate procedure to evaluate the weibull stress parameter 'm' and discussed the benefits of forecasting the specimen geometry dependency of CFT. Weibull stress parameter is estimated in their work with the values of CFT obtained from high fracture specimens. The estimate is based on a toughness scaling method that is widely used. Andrey P Jivkov, et al [11] applied LAF to compute the variations in the CFT due to the constraint and pre-staining effects. They present in their work about the analysis of CFT for dissimilar crack-tip constraints and dissimilar material conditions with and without pre-straining.

2. METHODOLOGY

Euro material A (22NiMoCr37) is used for both experimental and numerical analysis in this research, as it is a common material for pressure reactor vessels. The experimental dataset for Euro material A is available for the SENB specimen at -110°C for 2 different constraints named as SENB_0.5 $\left(\frac{a}{W} = 0.5\right)$, and SENB_0.2 $\left(\frac{a}{W} = 0.2\right)$, where 'a' and 'w' are width of the crack and specimen respectively in mm. The elastic-plastic properties of the Euro Material A at the temperature -110°C are obtained using the equations estimated by James et al [12].

$$E = -90T + 206000 \quad (1)$$

$$\sigma_y = 421.2 + 63.9\exp\left(-\frac{T}{91}\right) \quad (2)$$

$$\sigma_{UTS} = 564.1 + 70.2\exp\left(-\frac{T}{108}\right) \quad (3)$$

where E, σ_y, and σ_{UTS} represent the young' modulus, yield stress and the ultimate tensile strength respectively. The computed values are listed in table 1.

Table 1. Material properties of the SENB specimen at -110°C.

T(°C)	-110
$\boldsymbol{E(MPa)}$	215000
$\boldsymbol{\sigma_y(MPa)}$	612.96
$\boldsymbol{\sigma_{UTS}(MPa)}$	741.29

Two finite element models with varied crack lengths (a/w = 0.5), and (a/w = 0.2) are created in ABAQUS using the programmed script provided by Yankova et al [8]. The crack tip radius for temperature -110°C is selected to be roughly five times smaller than the crack tip opening displacement at the characteristic fracture toughness J_0, and a mesh with finite crack tip radius is created. The crack-tip radius has a paramount importance in the simulation procedure. The mesh in front of the tip may experience severe distortion when the radius is excessively small, which can result in program errors. Conversely, an oversized radius significantly deviates from reality and renders the simulation results meaningless. The crack-tip radius should be in the range of 1/3 to 1/5 of the crack tip opening displacement (CTOD) while the cleavage fracture occurs. Further, the crack tip

opening displacement (CTOD) can be found from the following critical J-Integral using the crack length a, thickness W, yield stress σ_y, and the ultimate tensile strength σ_{UTS} formulated as equations provided by ASTM.

$$J = n\sigma_y CTOD \tag{4}$$

where, $n = -0.111 + 0.817\frac{a}{W} + 1.36\frac{\sigma_{UTS}}{\sigma_y}$

Two methods are used to compute the weibull stress in this research. The original Beremin model method uses the standard procedure found in the literatures and a model proposed in this research incorporates a thinning coefficient θ, a function of temperature that indicates the conversion of brittle particles into cleavage initiators (CLS). The modified model [13] is completely based on the energy linked with creating kinks in dislocation lines. The thinning function describes about how the energy or the stress that is required for the kink formation changes as the material deforms.

The below equations show the kink formation free energy F_k and the critical length L^*, where the maximum shear stress is substituted using the Tresca criterion as an approximation to the Peierls stress.

$$F_k(\tau_{max}, T) = \tag{5}$$

$$\begin{cases} 0 & , \tau_{max} > \sigma_p(1 - T/T_{ath})^2 \\ U_k\left(1 - \frac{T}{T_{ath}} - \frac{\tau_{max}/\sigma_p}{1 - T/T_{ath}}\right), & \tau_{max} < \sigma_p(1 - T/T_{ath})^2 \end{cases}$$

$$L^*(\tau_{max}, T) = b\ exp\left[\frac{F_k(\tau_{max}, T)}{kT}\right] \tag{6}$$

where $F_k(\tau_{max}, T)$ is the kink-formation free energy and all other parameters are listed in table 2.

Table 2. Description of parameters used in the modified model.

Parameters	Values	Description
b	$0.248\ m$	Burger's vector of a screw dislocation
T_{ath}	$700\ K$	Athermal temperature
U_k	$0.33\ eV$	Zero-stress, Zero-temp kink-formation energy
σ_p	$900\ MPa$	Critical Peierls stress
k	$1.38x10^{-23}JK^{-1}$	Boltzmann constant
d	$10\ nm$	Mean inter-obstacle distance

The average space between carbides d is considered as the average displacement segment and thus the normalised free energy is given as

$$f_k(\tau_{max}, T) = \begin{cases} \frac{2F_k(\tau_{max}, T)}{kT}, & L > d \\ \frac{F_k(\tau_{max}, T)}{kT}, & L < d \end{cases} \tag{7}$$

Then depending on the normalised free energy, the thinning function θ for the Poisson process is given as,

$$\theta(\tau_{max}, T) = \frac{f_k(\tau_{max}, T)}{f_k(0MPa, -200℃)} \tag{8}$$

While merging the thinning function θ, the crack distribution is given as, $p(l) = \theta\frac{\alpha}{l^{\beta}}$, and thus the corresponding weibull stress can be expressed as,

$$\sigma_w = \sqrt[m]{\int \frac{\theta\sigma_1^m dV}{V_0}} \tag{9}$$

The thinning coefficient is inversely proportional to the temperature and thus, is constantly lesser than or equal to 1. When the thinning coefficient reaches the value 1, all the brittle particles are transferred into CLS, which usually occurs at very low temperature conditions. At higher temperatures the material becomes ductile and thus the fracture toughness increases. Eventually, the particles that are converted into CLS decreases. A standard model that could predict the fracture toughness for wide range of temperature and the geometry variation is the need of the hour. One of the aims of this research is to prove that the weibull stress calculated for the SENB with the modified model is equal to the value calculated using the original Beremin model.

The finite element (FE) analysis is performed and the elements within the fracture process zone (FPZ) are found for each load increment. The analysis is conducted based on two different conditions for the maximum principal stress and the corresponding plastic strain as usually applied in the local approaches to fracture,

$$\sigma_1 \geq \lambda\sigma_0 \quad \& \quad \varepsilon_{eq}^p \geq \varepsilon_{offset}^p \tag{10}$$

where λ is a scalar between 1 and 2.5, and ε_{offset}^p is equal to 0.2%. All elements in the FPZ have volumes

V and maximum and minimum primary stresses that are stored as arrays. The local approach is then applied as a post-processor to the FE data; for each increment, the processor loops over all load increments and compute the maximum shear stress based on the Tresca criterion, the kink-formation free energy, characteristic length scale, the normalised free energy, the thinning function, and the maximum principal stress within the load history up to the current increment. Then using any form parameter m and unit volume V, the Weibull stress is calculated. For different temperatures, the weibull stress curves as a function of J is plotted the characteristic J at 63.2% is calculated. This article focuses on the numerical analysis at -110°C.

The experimental data shown in figure 1(a) represents the scatter of the fracture toughness K_{JC} at -100°C for a high constraint (a/W = 0.5) and a low constraint (a/W = 0.2) specimen. The temperature and the geometry are chosen according the available experimental dataset. Figure 1(b) represents the cumulative distribution function of the fracture toughness at -100°C for both the constraints. The CDF curves provide insights into the likelihood of observing fracture toughness values below or above a certain threshold for each constraint level. The average fracture toughness values and their variability between the constraint levels could vary depending on the distribution of the scatter plot and the shape of the CDF curves. Higher variability if observed when a flatter CDF curve of a wider is present, whereas a steeper CDF curve or a narrower scatter might suggest more consistent performance.

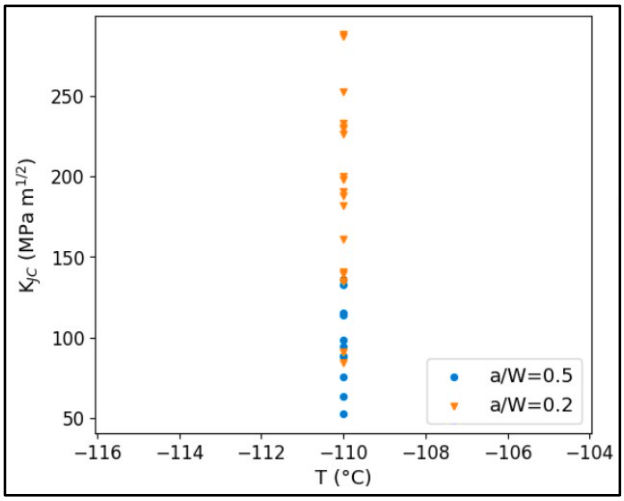

Fig. 1(a). Scatter of Fracture toughness at -110°C for a/W = 0.5 & 0.2.

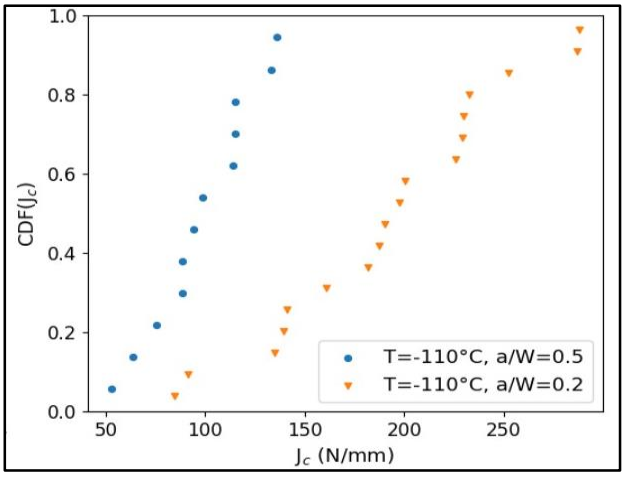

Fig. 1(b). Cumulative distribution function of the fracture toughness.

Figure 2 represents the curve fit of the cumulative distribution function. The point '0.632 quantile' is used to identify the median time to failure in systems. Thus the J_C values for both high and low constraints could be easily formulated from the above plots.

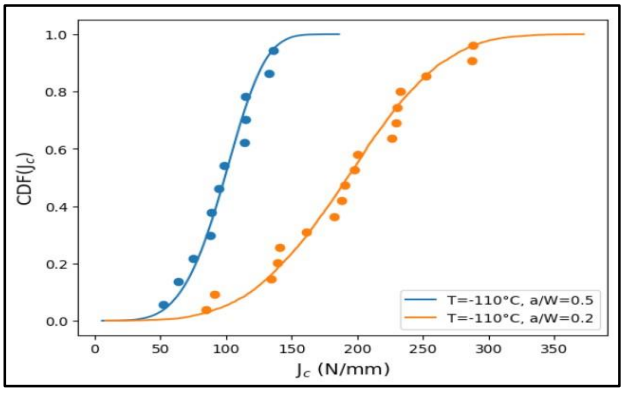

Fig. 2. Curve fit plot for a/W = 0.5 & 0.2 at -110°C.

Table 3 represents the maximum J_0 and the J_0 at 0.632 quantile for both high and low constraints from the cumulative distribution.

Table 3. Maximum $\boldsymbol{J_0}$ and $\boldsymbol{J_0}$ at 0.632 quantile from the cumulative distribution function.

a/W	0.5	0.2
$\boldsymbol{J_0^{max}}$ $\boldsymbol{(N/mm)}$	136.0	288.1
$\boldsymbol{J_0^{0.632}}$ $\boldsymbol{(N/mm)}$	107.339	213.034

Finite Element Analysis is conducted for the SENB specimen as per the boundary conditions. Both the low and high constraint specimens are simulated using the ABAQUS software the respective stress contour plots are represented in figures 3 & 4 which also show the details of the element mesh near the crack tip region and alongside the crack propagation path for high and low constraint respectively.

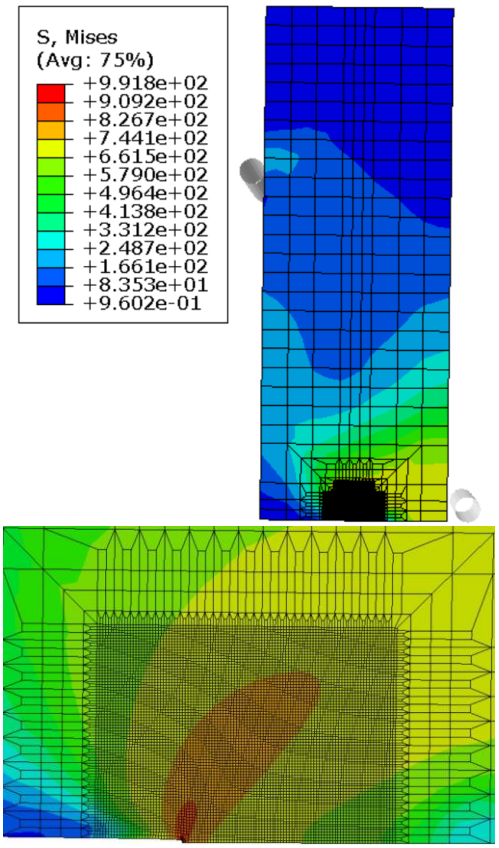

Fig. 3. Stress contour of SENB specimen with high constraint.

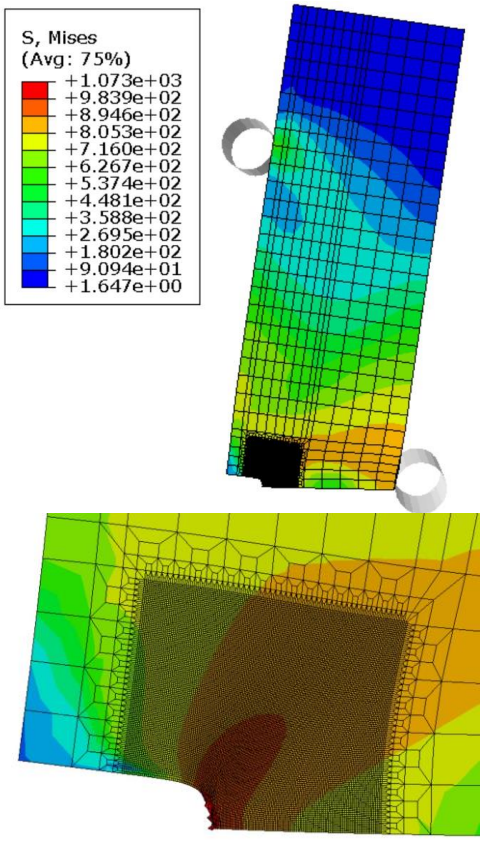

Fig. 4. Stress contour of SENB specimen for low constraint.

In the postprocessing, the necessary information for J integral calculation is extracted by setting up appropriate output request. This involved selecting the crack tip elements, integration points and specifying the appropriate output variables (stress components, displacements, etc). The characteristic J_0 is extracted and presented in table 4 for both high and low constraints at -110°C. The maximum yield stress from the numerical analysis is found to 635.20 MPa for both the geometries.

Table 4. Characteristic J_0 from the finite element analysis.

a/W	0.5	0.2
J_0 (N/mm)	107.236	214.370

Both situations a/W = 0.5 & 0.2 exhibit close agreement between experimental and numerical results. This indicates that the material's behaviour under the specified loading circumstances is accurately predicted by the numerical analytical approach used. The minimal difference between experimental and numerical data shows how accurate the finite element analysis technique is in this investigation. The slight discrepancies can be the result of measurement, production flaws, and material property variability. Greater crack tip deformations and faster energy release rates are typically associated with shorter cracks, which also frequently associated with higher stress concentration.

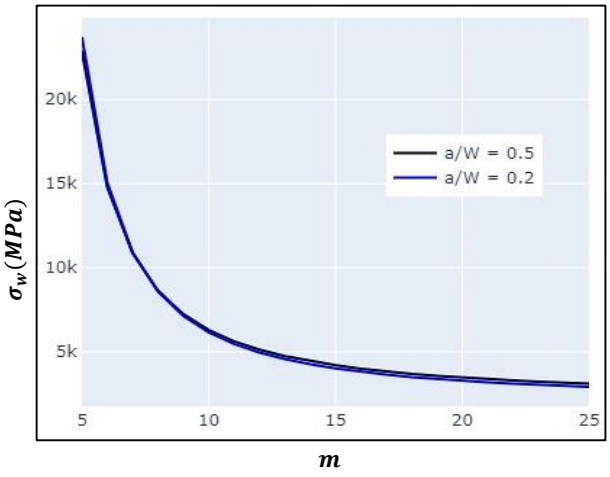

Fig. 5. σ_w vs m plot from the original model for a/W = 0.5 & 0.2

A smaller m denotes a uniform distribution of defect sizes in the context of CFT, resulting in a more deterministic and consistent Weibull stress σ_w. On the other hand, a larger m denotes a more

dispersed fracture toughness response due to a wider variety of defect sizes, causing the Weibull stress to become less predictable. Thus, the relation is defined using both the original Beremin model and the modified model, in order to calculate the suitable shape parameter for the analysis. Figure 5 represents the plot between the Weibull stress σ_w and the shape parameter m for both the low and high constraint specimens calculated using the original Beremin model.

Figure 6 represents the plot between percentage difference in the Weibull stress $\Delta\sigma_w$ and the shape parameter m for both low and high constraint using the original Beremin model.

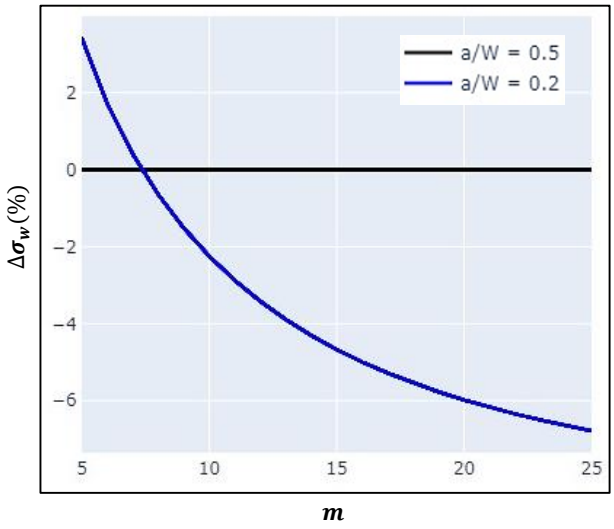

Fig. 6. $\Delta\sigma_w$ vs m plot from the original model for a/W = 0.5 & 0.2

Figure 7 represents the plot between the Weibull stress σ_w and the shape parameter m for both the low and high constraint specimens calculated using the modified Beremin model.

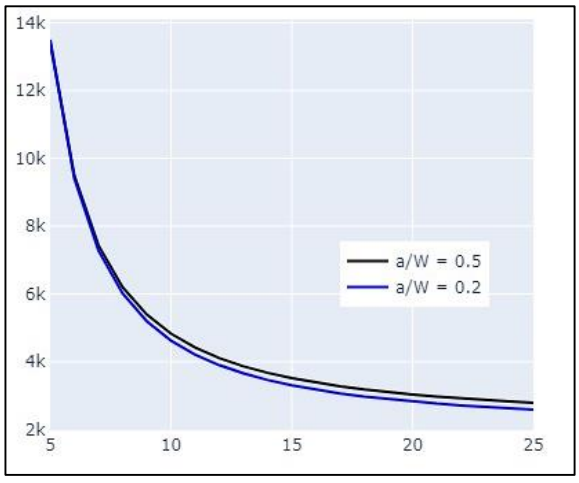

Fig. 7. σ_w vs m plot from the modified model for a/W = 0.5 & 0.2

Figure 8 represents the plot between percentage difference in the Weibull stress $\Delta\sigma_w$ and the shape parameter m for both the low and high constraint using the modified Beremin model.

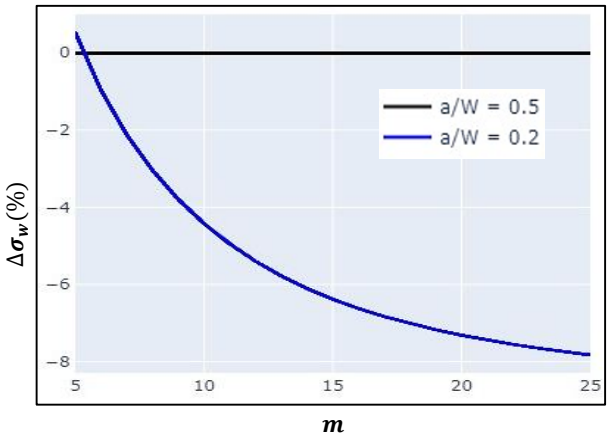

Fig. 8. $\Delta\sigma_w$ vs m plot from the modified model for a/W = 0.5 & 0.2

In predicting the effect of geometry on CFT, the Weibull stresses for both high and low constraints are very well fitted. Both the high and low constraint specimens have almost equal Weibull stresses at shape parameter $m = 15$ for the original Beremin model. With a 5.5% difference in the similarity of the Weibull stresses, the shape parameter $m = 11$ seems to work for the both the constraints using the modified model. Tables 5 & 6 show the Weibull stresses for the average shape parameters for the original and modified models respectively.

Table 5. Weibull stresses for the corresponding average shape parameter $\boldsymbol{m}$ from the original model.

a/W	0.5	0.2
Average $\boldsymbol{m}$	15	15
$\boldsymbol{\sigma_w}$ $(\boldsymbol{MPa})$	4318.049	4390.880

Table 6. Weibull stresses for the corresponding average shape parameter $\boldsymbol{m}$ from the modified model

a/W	0.5	0.2
Average $\boldsymbol{m}$	11	11
$\boldsymbol{\sigma_w}$ $(\boldsymbol{MPa})$	4206.569	4108.958

This section presents the J-Integral predicted based on the original Beremin model and the modified model. Figures 9 & 10 represent the plot between the weibull stress σ_w and the J-integral for the high constraint specimen. Similarly, figures 11 & 12 represent the plot among the weibull stress σ_w and the J-integral for the low constraint specimen. Using the calculated weibull stress with corresponding shape parameters, the prediction based on $J_0^{T=-110°C}$ is plotted.

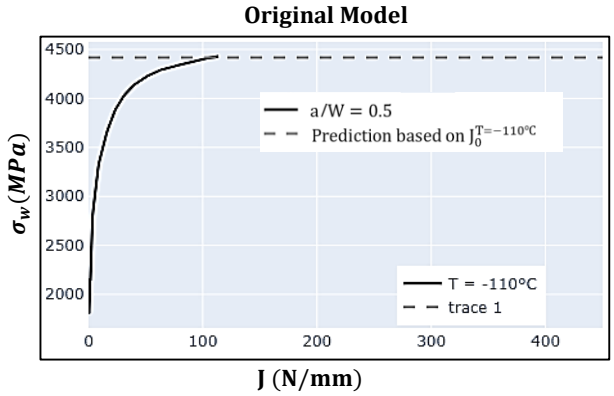

Fig. 9. σ_w vs J-Integral plot from original model for a/W = 0.5.

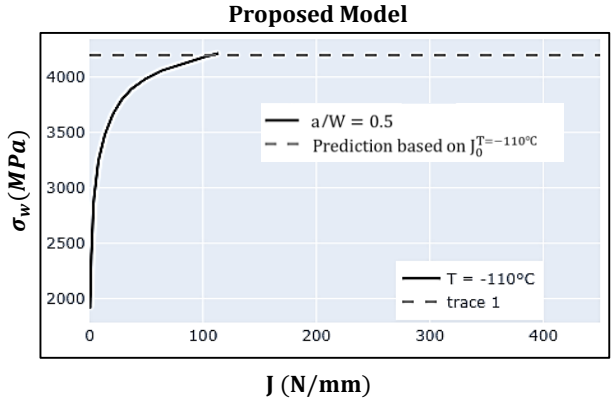

Fig. 10. σ_w vs J-Integral plot from modified model for a/W = 0.5.

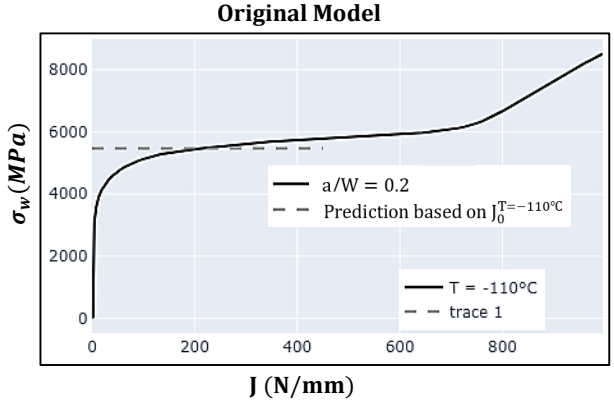

Fig. 11. σ_w vs J-Integral plot from original model for a/W = 0.2.

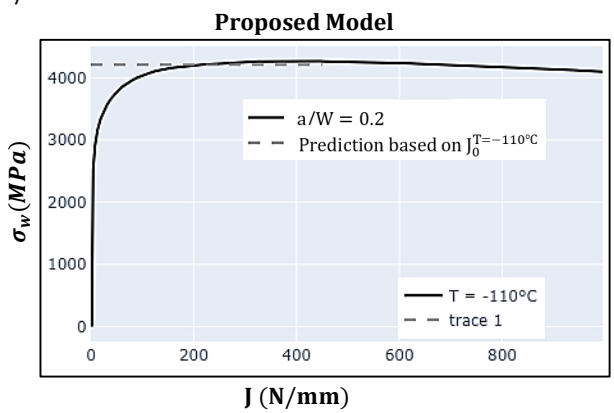

Fig. 12. σ_w vs J-Integral plot from modified model for a/W = 0.2.

Table 7 & 8 show the calculated J-Integral using both original and modified models for both high and low constraints respectively.

Table 7. Prediction based on $\mathbf{J_0^{T=-110°C}}$ using original and modified model for $\mathbf{a/W = 0.5}$.

$\mathbf{a/W = 0.5}$	$\mathbf{J_0^{T=-110°C}}$ N/mm
Original Beremin Model	108.13
Modified Beremin Model	107.82

Table 8. Prediction based on $\mathbf{J_0^{T=-110°C}}$ using original and modified model for $\mathbf{a/W = 0.2}$.

$\mathbf{a/W = 0.2}$	$\mathbf{J_0^{T=-110°C}}$ N/mm
Original Beremin Model	217.64
Modified Beremin Model	214.37

Notable conclusions are found when comparing the prediction efficacy of numerical analysis to experimental results for fracture toughness. Particulary, both the original and proposed models show an advantageous alignment with fracture toughness values when studying high constraint specimens. Notably, the modified model has an exceptional low variation of just 0.4% demonstrating its strong prediction skills. The original model diverges from the experimental data in the case of low constraint specimen by about 2%, whereas the modified model shows much increased accuracy with only a 0.5% variance.

Furthermore, it is important to underscore the enhanced accuracy of the modified model in relation to envisaging the fracture toughness with varied geometries of the SENB specimen. The model's adjustments appear to have a noticeable effect on its prediction and the improved appropriateness of the model is highlighted by the reduced discrepancies seen across specimens of high and low constraints. Also, it is certainly unreasonable to state that the modified model is compatible to every other geometry of the SENB specimen, as the present study is limited to only two geometries at -110°C. Both the original and the proposed model are investigated using various shape parameters in order to have the exact experimental fracture toughness for the known geometry. In such case, m = 8 & 5, worked for both the original and modified models respectively and thus the prediction of unknown geometries is analysed. Figures 13 & 14 represent the plot between the Weibull stress and the J-Integral using the predictions based on the known geometries of both the original and modified model respectively.

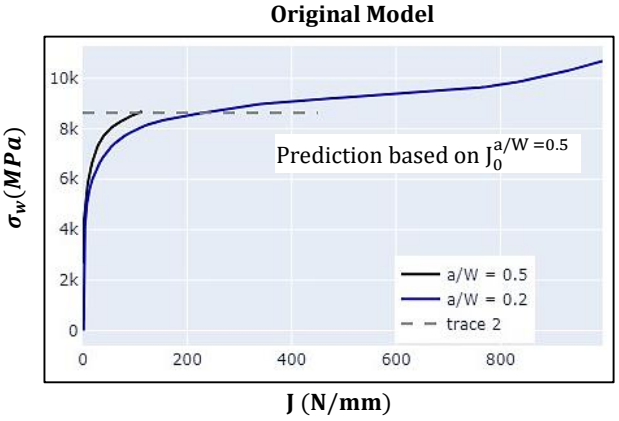

Fig. 13. Prediction of σ_w vs J-Integral plot from original model.

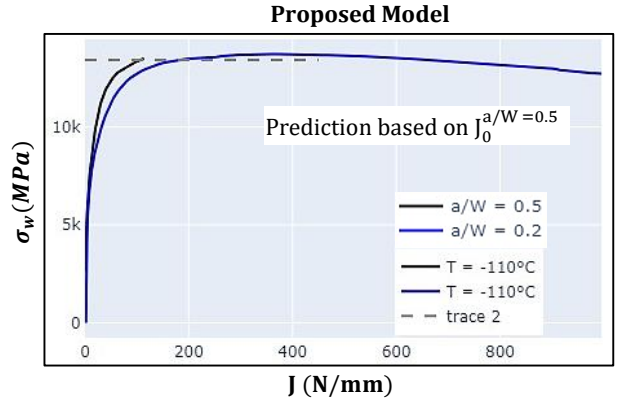

Fig. 14. Prediction of σ_w vs J-Integral plot from modified model.

Tables 9 & 10 represent the predictions of unknown geometry using both the original and modified model respectively.

Table 9. Prediction based on the known $\boldsymbol{J_0}$ using the original model.

a/W	$J_{0.632}^{a/W=0.5}$ (N/mm)	$J_{0.632}^{a/W=0.2}$ (N/mm)
0.5	-	109.21
0.2	224. 27	-

Table 10 Prediction based on the known $\boldsymbol{J_0}$ using the modified model.

a/W	$J_{0.632}^{a/W=0.5}$ (N/mm)	$J_{0.632}^{a/W=0.2}$ (N/mm)
0.5	-	101.92
0.2	199.75	-

Using the original model, there is a 5.3% error in the prediction of low constraint specimen using the original model, whereas there is a 7% error while using the modified model. Also, the error percentage while predicting the high constraint specimen using original model is lesser than 2%, and using the modified model is around 5.08%. Numerical simulations must take the effect of mesh size on SENB into account in a significant way. The accuracy of fracture mechanics assessments can be considerably impacted by the mesh size selection. By capturing localised stress fluctuations, a finer mesh improves accuracy, while a coarser mesh may produce inaccurate predictions of crack propagation and fracture behaviour. When examining the impact of mesh size on SENB specimen simulations, striking a balance between computational efficiency and predicted accuracy remains a major problem.

Tables 11 & 12 show the variations of J-Integral with the mesh size for a/W = 0.5 using the original and the modified model.

Table 11. Variation of J-Integral with the mesh size for $\mathbf{a/w = 0.5}$ using the original model.

Mesh size (μm)	$\boldsymbol{m}$	$J_0^{T=-110°C}$ N/mm
100	15	108.13
50	17	109.43
30	18	109.91

Table 12. Variation of J-Integral with the mesh size for $\mathbf{a/W = 0.5}$ using the modified model.

Mesh size (μm)	$\boldsymbol{m}$	$J_0^{T=-110°C}$ N/mm
100	11	107.82
50	13	108.53
30	16	109.90

The prediction by both the models for a/W = 0.5 is not considerably influenced and the projected fracture toughness with difference mesh sizes varies less than 2% for both the original and modified models.

Tables 13 & 14 show the variations of J-Integral with the mesh size for a/W = 0.2 using the original and the modified model.

Table 13. Variation of J-Integral with the mesh size for $\mathbf{a/W = 0.2}$ using the original model.

Mesh size (μm)	$\boldsymbol{m}$	$J_0^{T=-110°C}$ N/mm
100	15	217.64
50	17	219.05
30	18	219.83

Table 14. Variation of J-Integral with the mesh size for $\mathbf{a/W = 0.2}$ using the modified model.

Mesh size (μm)	$\boldsymbol{m}$	$J_0^{T=-110°C}$ N/mm
100	11	214.37
50	14	216.71
30	18	219.50

Similarly, the prediction by both the models for $a/W = 0.2$ is still not significantly influenced by the mesh size and the predicted fracture toughness with difference mesh sizes does not vary more than 3% for both original and modified models. It is also observed that the σ_w vs J-Integral plot does not show any variation, proving the fact that the mesh size has very little effect on the prediction accuracy.

3. CONCLUSION

The research reported in this article investigated the effects of geometry on the fracture toughness by using the proposed model. The research focused on the SENB specimen at -110°C for two different constraints ($a/W = 0.2$ & 0.5). The prediction of the fracture toughness using both the original and proposed model was performed on both the specimens and the fracture toughness of $a/W = 0.2$ based on the known properties of $a/W = 0.5$. The effect of mesh size on the prediction accuracy was also analysed.

The major findings of the study are summarized below:

- Both the original and the modified models are able to analyse the effects of geometry on the fracture toughness for both $a/W = 0.2$ & 0.5 with a single shape parameter at -110°C.
- Excellent agreement is shown between the experimental and the predicted characteristic fracture toughness at -110°C.
- The fitted probability distributions show good agreement between the prediction and the experimentation at -110°C
- The developed model could be extensively used in predicting the fracture toughness at various geometries with just the experimental fracture toughness at a known geometry and temperature.
- The mesh size has almost no effect on the prediction results.
- The prediction analysis of $a/W = 0.2$, based on the known properties of $a/W = 0.5$ resulted in a satisfactory manner for both the original and the modified models.

REFERENCES

[1] D. K. Duraivelu and K. S. Rao, "ProducQual – A Conceptual Model for Quality Gap Analysis Across PLC," *Journal of the Indian Institute of Science*, vol. 86, no. 2, pp. 113–124, Mar. 2006.

[2] F. M. Beremin, A. Pineau, F. Murdy, J. C. Devaux, Y. D'Escatha, and P. Ledermann, "A Local Criterion for Cleavage Fracture of a Nuclear Pressure Vessel Steel," *Metallurgical Transactions A*, vol. 14, pp. 2277–2287, 1983, doi: 10.1007/BF02663302.

[3] J. P. Petti and R. H. Dodds, "Calibration of the Weibull Stress Scale Parameter, σμ Using the Master Curve," *Engineering Fracture Mechanics*, vol. 72, pp. 91–120, 2005, doi: 10.1016/j.engfracmech.2004.03.009.

[4] X. Zhao et al., "Introducing Heterogeneity into Brittle Fracture Modeling of a 22NiMoCr37 Ferritic Steel Ring Forging," *Journal of ASTM International*, 2008, doi: 10.1520/JAI101562.

[5] V. S. Barbosa and C. Ruggieri, "A Simplified Estimation Procedure for the Weibull Stress Parameter, m, and Applications to Predict the Specimen Geometry Dependence of CFT," *International Journal of Pressure Vessels and Piping*, vol. 188, p. 104228, 2020, doi: 10.1016/j.ijpvp.2020.104228.

[6] C. Ruggieri, X. Gao, and R. H. Dodds, "Calibration of Weibull Stress Parameters Using Fracture Toughness Data," *International Journal of Fracture*, vol. 92, pp. 175–200, 1998, doi: 10.1023/A:1007521530191.

[7] A. Andrieu, A. Pineau, J. Besson, D. Ryckelynck, and O. Bouaziz, "Beremin Model: Methodology and Application to the Prediction of the Euro Toughness Data Test," *Engineering Fracture Mechanics*, vol. 95, pp. 102–117, 2012, doi: 10.1016/j.engfracmech.2011.10.019

[8] M. S. Yankova, A. P. Jivkov, R. Patel, and A. H. Sherry, "Capturing the Temperature Dependence of Cleavage Fracture-Toughness in the Ductile-to-Brittle Transition Regime in Ferritic Steels Using an Improved Engineering Local Approach," *Journal of Pressure Vessel Technology*, vol. 144, p. 031503, 2022, doi: 10.1115/1.4054497

[9] C. Ruggieri and A. P. Jivkov, "A Probabilistic Approach for Cleavage-Fracture Including the Statistics of Micro-Cracks: Application to a Reactor Pressure Vessel Steel," *Engineering Fracture Mechanics*, vol. 272, p. 108702, 2022, doi: 10.1016/j.engfracmech.2022.108702

[10] V. S. Barbosa and C. Ruggieri, "A Simplified Estimation Procedure for the Weibull-Stress Parameter and Applications to Predict the Specimen Geometry Dependence of Cleavage Fracture-Toughness," *International Journal of Pressure Vessels and Piping*, vol. 188, pp. 15–25, 2020, doi: 10.1016/j.ijpvp.2020.104228

[11] A. P. Jivkov et al., "Use of Local Approaches to Calculate Changes in Cleavage Fracture-Toughness Due to Pre-Staining and Constraint Effects," *Material Science: Theoretical and Applied Fracture Mechanics*, vol. 104, pp. 1–12, 2019, doi: 10.1016/j.tafmec.2019.102380

[12] P. M. James, M. Ford, and A. P. Jivkov, "A Novel Particle Failure Criterion for Cleavage Fracture Modelling Allowing Measured Brittle Particle Distributions," *Engineering Fracture Mechanics*, vol. 121, pp. 98–115, 2014, doi: 10.1016/j.engfracmech.2014.03.005

[13] J. Pan and M. Yin, "A Study on Fracture Toughness Based on a Modified Beremin Model," *Journal of Materials Engineering and Performance*, vol. 30, pp. 8309–8321, 2021, doi: 10.1007/s11665-021-06072-w